Front. Optoelectron.
https://doi.org/10.1007/s12200-018-0772-6

REVIEW ARTICLE

On-chip silicon polarization and mode handling devices

Yong ZHANG, Yu HE, Qingming ZHU, Xinhong JIANG, Xuhan Guo, Ciyuan QIU, Yikai SU (✉)

State Key Lab of Advanced Optical Communication Systems and Networks, Department of Electronic Engineering, Shanghai Jiao Tong University, Shanghai 200240, China

Abstract Mode- and polarization-division multiplexing are new promising options to increase the transmission capacity of optical communications. On-chip silicon polarization and mode handling devices are key components in integrated mode- and polarization-division multiplexed photonic circuits. In this paper, we review our recent progresses on silicon-based polarization beam splitters, polarization splitters and rotators, mode (de) multiplexers, and mode and polarization selective switches. Silicon polarization beam splitters and rotators are demonstrated with high extinction ratio, compact footprint and high fabrication tolerance. For on-chip mode multiplexing, we introduce a low loss and fabrication tolerant three-mode (de)multiplexer employing sub-wavelength grating structure. In analogy to a conventional wavelength selective switch in wavelength-division multiplexing, we demonstrate a selective switch that can route mode- and polarization-multiplexed signals.

Keywords silicon photonics, polarization beam splitter, polarization splitter and rotator, mode (de)multiplexer, selective switch

1 Introduction

Optical communication technologies have made many breakthroughs to support the increasing information capacity in the past decade. The transmission capacity of a single fiber increases by ten times every four years [1]. Multiple dimensions of an optical carrier, including time, frequency, phase, mode and polarization, can be employed to carry optical data. Recently, as a new dimension, space has been explored to increase the data-carrying capacity [2]. Much progress has been made, including space-division multiplexing (SDM) in multi-core fibers [1,3] and mode-division multiplexing (MDM) in few-mode fibers [4,5]. The transmission capacity of a single fiber can be increased significantly when combining the five multiplexing dimensions.

Photonic integrated circuits are promising schemes in optical communication systems [6]. Integrated photonic devices can be fabricated on many material platforms, such as silicon [7], Si_3N_4 [8], silica [9], InP [10], GaAs [11], and $LiNbO_3$ [12]. In recent years, silicon photonics has become one of the most promising platforms for photonic integration due to the advantages of low cost, low power consumption, compact footprint, high level of integration, and compatibility with mature complementary metal oxide semiconductor (CMOS) processes [13]. Many impressive silicon passive and active devices have been achieved, including on-chip lasers [14,15] and sources [16,17], modulators [18], switches [19], filters [20,21], interleavers [22], diodes [23], and photodetectors [24]. Photonic integrated MDM and polarization-division multiplexing (PDM) technologies have attracted much attention in the past years [25]. On-chip polarization and mode handling devices are key components, including polarization beam splitter (PBS), polarization rotator (PR), polarization splitter and rotator (PSR), mode (de)multiplexer, mode and polarization switch, and so on.

In this paper, we review our recent work on silicon polarization and mode handling devices. In Section 2, silicon-based PBS, PR and PSR devices will be discussed. A PBS is used to separate an input light to two orthogonal polarized beams (TE and TM). A high-extinction-ratio grating-based PBS and a bridged-bent-coupler-based PBS will be shown in Section 2.1. An ultra-compact bent-coupler-based PSR and a large tolerance subwavelength-grating-based PSR will be introduced in Section 2.2. Low loss and large tolerance mode multiplexers are key devices in MDM schemes. A silicon three-mode (de)multiplexer employing subwavelength grating will be discussed in

Received November 24, 2017; accepted December 27, 2017

E-mail: yikaisu@sjtu.edu.cn

Invited, Wuhan Optoelectronics Forum (WHOF) 118

Section 3. In analogy to a conventional wavelength selective switch (WSS) that routes any wavelength channel from one input port to any output port, a switch that can route mode- and polarization-multiplexed signals can effectively increase the capacity and add new functionalities. We demonstrate an on-chip silicon 2 × 2 mode- and polarization-selective switches (MPSS) operating on one wavelength in Section 4.

2 Silicon polarization handling devices

Polarization handling devices, including PBSs, PRs and PSRs, are widely used in the PDM systems. They are also key components in the polarization-diversity scheme, which is a general solution to eliminate the polarization sensitivity of silicon waveguide devices [26]. Polarization-diversity scheme has many important applications, such as in coherent receiver systems [27,28].

2.1 Polarization beam splitters

A PBS is a basic building block for polarization controlling. Many schemes were proposed to realize PBS devices, including multimode interference (MMI) structures [29,30], photonic crystal [31], out-of-plane grating [32], hybrid plasmonic waveguides [33,34], directional couplers (DCs) [35,36], and so on. We introduce two kinds of on-chip PBSs in the following.

2.1.1 High-extinction-ratio grating-based PBS [37]

Polarization extinction ratios (PERs) are important for a PBS, and typically at least 30 dB are needed in the practical applications [38]. A compact PBS based on asymmetrical grating-assisted contradirectional couplers (GACCs) was theoretically proposed [39]. An advantage of such PBS is that it does not require stringent phase matching and coupling length conditions. We performed a detailed study of a high-extinction-ratio PBS in terms of design, fabrication, and tolerance to width and coupling length variations. Figures 1(a) and 1(b) show the schematic structure for the proposed GACC-based PBS. The device consists of two parallel silicon strip waveguides, A and B. The corrugations on the sidewall of the two waveguides are designed to form grating structures. The sidewall grating is designed to enhance the contra-directional coupling of the TE polarization, but has no effect on the coupling of the TM polarization. Therefore, a TE-polarized light is contra-directionally coupled from waveguide A to waveguide B by the periodic corrugations. High-efficiency TE-polarized light output is obtained in the Cross port. A TM-polarized light goes through waveguide A without coupling. High-efficiency TM-polarized light outputs at the Thru port.

The period and the duty cycle of the corrugations are Λ = 344 nm and 52%, respectively. The corrugation widths on waveguide A and waveguide B are ΔW_A = 137 nm and ΔW_B = 123 nm, respectively. The gap between the waveguides is 65 nm. The coupling length of the two waveguides is determined by the period Λ and corrugation period numbers N. Figures 1(c) and 1(d) show the power distributions in the PBS structure for the TE- and TM-polarized light inputs, respectively, which are calculated by three-dimensional finite-difference time-domain (3D FDTD) method. The simulation results show that the TE- and TM-polarized light signals are separated by the grating structure effectively. Figure 2 shows the scanning electron microscope (SEM) images of a fabricated PBS with a corrugation period number N = 80.

In the measurements, the TE- and TM-polarized lights from a tunable laser (Keysight 81960A) were coupled into/out of the chip by grating couplers. The output spectra

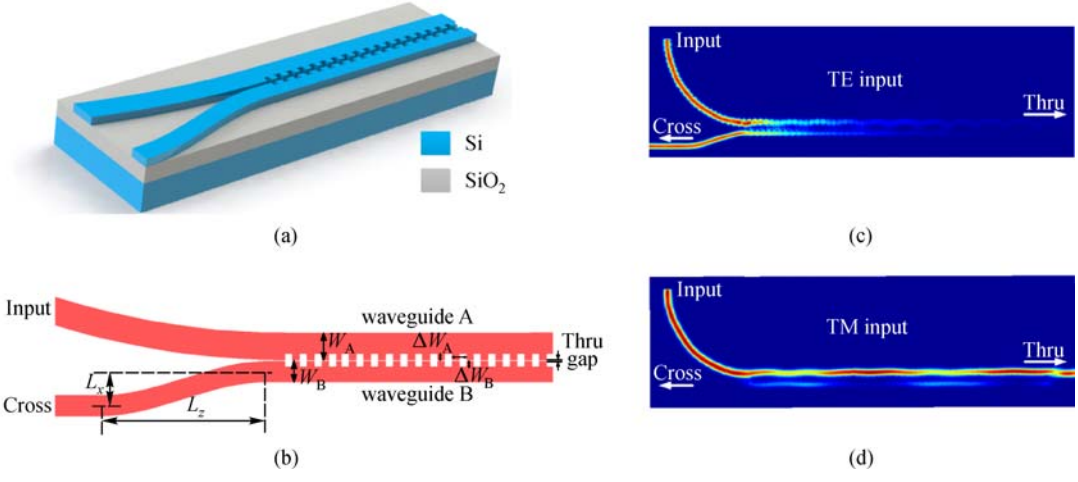

Fig. 1 Schematic structure of the proposed GACC-based PBS. (a) 3D view; (b) top view. Simulated power distributions for (c) TE-polarized light inputs, (d) TM-polarized light inputs [37]

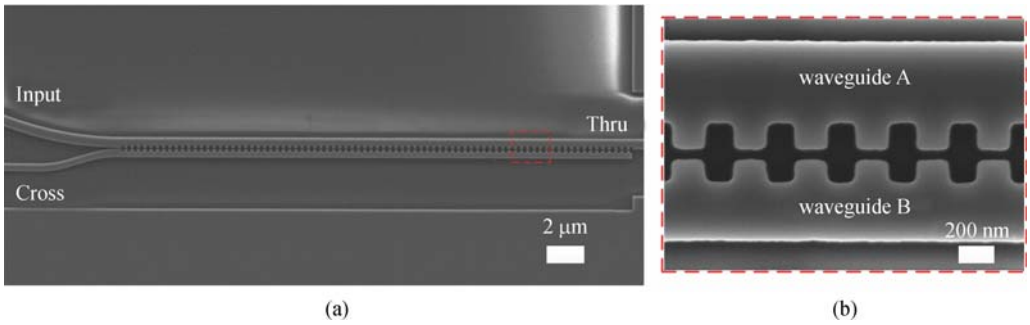

Fig. 2 (a) SEM image of a fabricated GACC-based PBS with corrugations period number $N = 80$; (b) magnified micrograph of the gratings [37]

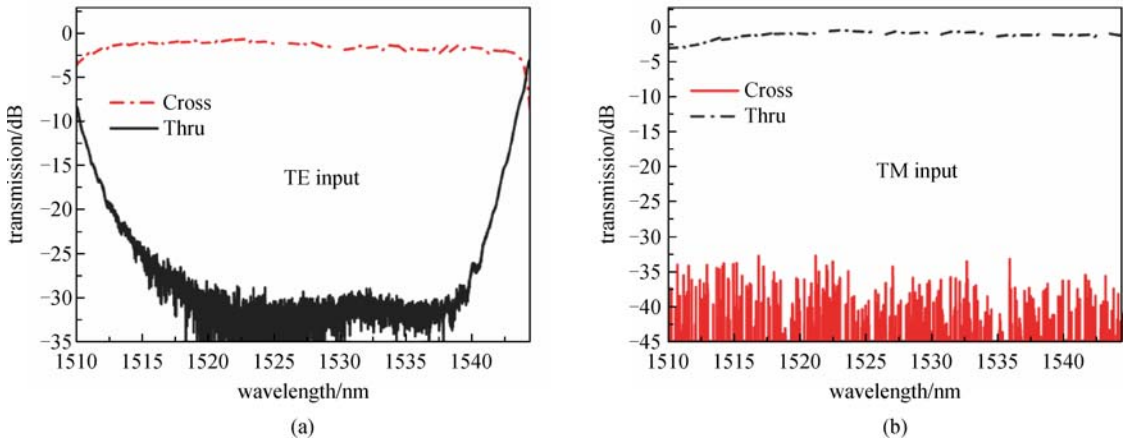

Fig. 3 Measured transmission responses at the Cross and Thru ports for (a) TE-polarized and (b) TM-polarized light inputs, respectively [37]

were recorded by an optical spectrum analyzer (OSA) (Yokogawa AQ6370B). The grating couplers exhibit a significant polarization dependence. Figure 3 illustrates the measured transmission responses at the Cross and Thru ports of a fabricated PBS for the TE- and TM-polarized input signals, respectively. The corrugation period numbers N is 80, and the corresponding coupling length is 27.52 μm. The responses are normalized to the transmission of a grating-coupled straight waveguide. For the TE-polarized light input, the PER is higher than 30 dB in the wavelength range of 1517 – 1538 nm, and the insertion loss is less than 1 dB. For the TM-polarized light input, the PER is higher than 30 dB in the wavelength range of 1517 – 1544 nm, and the insertion loss is less than 1 dB. The operation wavelength can be finely tuned by changing the corrugation period and the width. Wider operation bandwidth could be realized by applying larger refractive-index perturbation and stronger coupling [39].

2.1.2 PBS based on a bridged bent coupler [40]

Figures 4(a) and 4(b) show the schematic structure of a proposed PBS based on a bridged asymmetrical bent directional coupler. To achieve high PER and broad operation bandwidth, a parallel bridged waveguide is placed in a conventional bent directional coupler. The three bent waveguides have different core widths of w_1, w_2 and w_3, respectively. The phase-matching condition is satisfied for the coupling of TM polarization between the three bent waveguides. Therefore, the TM-polarized light is coupled from the Input port to the Cross port. On the other hand, the phase-matching condition is not satisfied due to the birefringence of the silicon waveguides for the TE polarization. The TE-polarized light goes through the input waveguide directly and outputs at the Bar port. The bending radius of waveguide 1 (WG 1) is $R_1 = 20$ μm. The arc-angle of the coupling region is 0.1π rad, and the corresponding coupling length is 6.28 μm. Figures 4(c) and 4(d) show the simulated power distributions for the TE- and TM-polarized light inputs, respectively. The simulated results show that, the TM-polarized light is coupled and outputs from the Cross port, while the TE-polarized light goes through the waveguide directly and outputs from the Bar port.

Figure 5(a) shows a SEM photo of a fabricated PBS. Figures 5(b) and 5(c) show the measured transmission

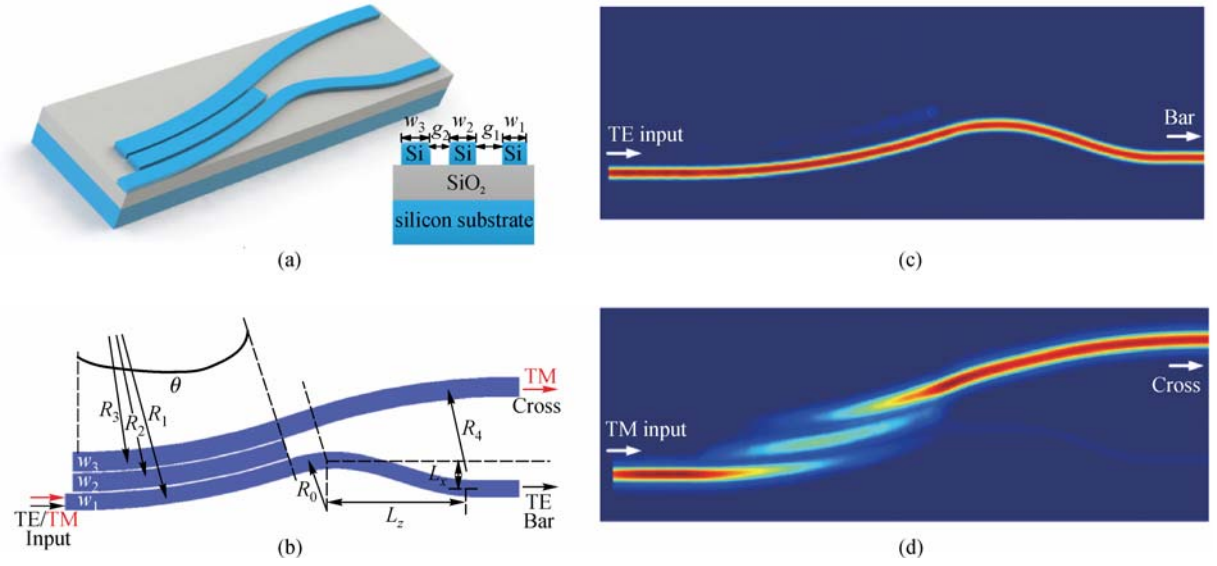

Fig. 4 (a) and (b) Schematic structure of the proposed bridged bent coupler PBS; (c) and (d) simulated power distributions in the PBS for the TE- and TM-polarized light inputs, respectively [40]

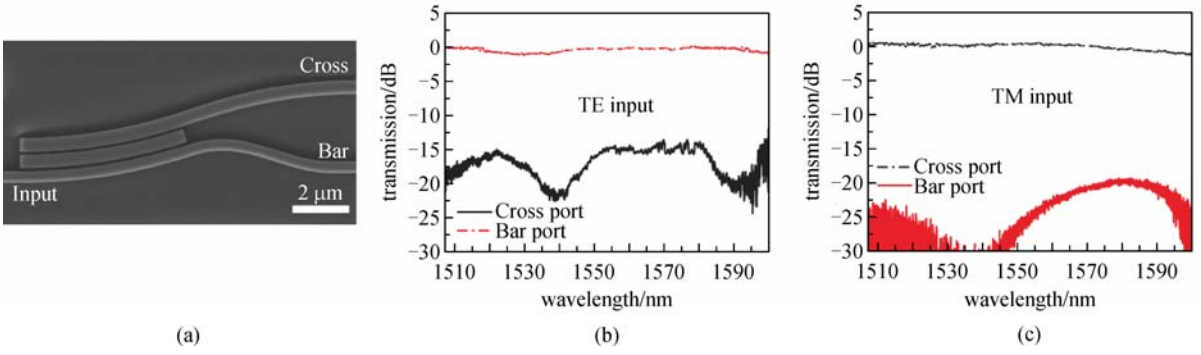

Fig. 5 (a) SEM photo of a fabricated PBS based on a bridged bent directional coupler. Measured transmission responses at the Bar and Cross ports for (b) TE-polarized and (c) TM-polarized light inputs [40]

responses at the Bar and Cross ports of the fabricated PBS when the TE- and TM- polarized lights are injected, respectively. For the TE-polarized light input, high-efficiency TE-polarized light output is obtained at the Bar port. The PER is higher than 15 dB in a broad wavelength range of 1507 – 1600 nm, and the insertion loss is < 1 dB. For the TM-polarized light input, the PER is higher than 20 dB in the wavelength range of 1507 – 1600 nm, and the corresponding insertion loss is < 1 dB in the broad wavelength range.

2.2 Polarization splitters and rotators

Polarization splitting and rotating can be achieved simultaneously in a PSR device, which works as a PBS cascaded with a PR. When the vertical and horizontal symmetry is broken and if two orthogonal modes have equal effective refractive indices and optical paths, cross-polarization coupling occurs, and one polarization can be effectively converted to the other one [41]. Many types of silicon-waveguide PSRs have been reported based on various structures, including directional coupler [42,43], MMI [30], Y-junctions [44], and so on. We discuss two kinds of PSRs in the following.

2.2.1 Silicon PSR based on a bent directional coupler [45]

Figures 6(a) and 6(b) show the schematic structure of the proposed PSR device. It consists of two parallel silicon bent waveguides (WG 1 and WG 2) coupled to each other. To achieve an efficient TM-TE cross-polarization conversion, air, which is different from the bottom silicon oxide layer, is adopted as the top cladding. The widths of the two bent waveguides are optimized so that the fundamental TM

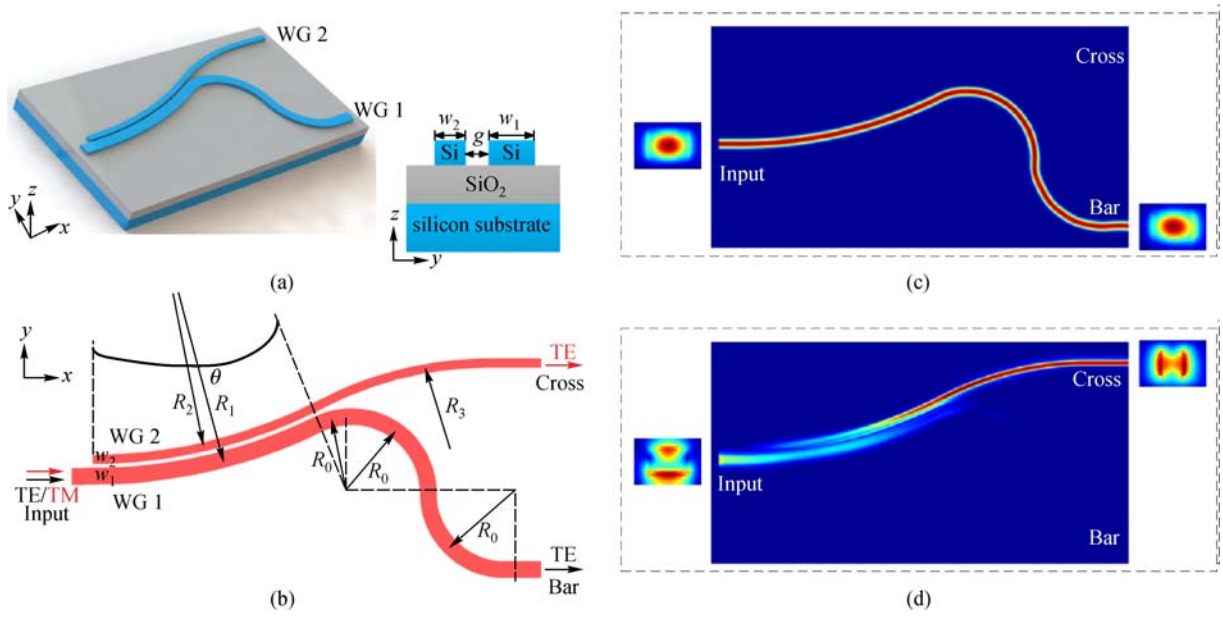

Fig. 6 Schematic structure of the proposed silicon PSR based on a bent directional coupler. (a) 3D view; (b) top view. (c) and (d) Simulated power distributions at the plane of $z = 0$ for the TE- and TM-polarized light inputs, respectively. The four insets depict the mode distributions at the cross section of yz of Input and Output ports [45]

mode in WG 1 and the fundamental TE mode in WG 2 have equal optical path lengths, i.e., the phase matching condition is satisfied. In this case, an efficient TM-TE cross-polarization coupling occurs between the two bent waveguides. The TM-polarized light in WG 1 is coupled to WG 2 and is simultaneously converted to the TE-polarized light. TE-polarized light outputs at the Cross port. On the other hand, due to the birefringence of the silicon nano-waveguides, the phase matching condition cannot be satisfied between the TE mode in WG 1 and any guided mode in WG 2. Thus, the TE-polarized light goes through WG 1 without coupling and outputs at the Bar port.

The angle θ of the coupling region is optimized to be 26°, and the corresponding coupling length is $L_c = R_1 \sin(\theta) = 8.77$ μm. Figures 6(c) and 6(d) depict the simulated power distributions at the plane of $z = 0$ for the TE- and TM-polarized light inputs, respectively. The simulation results show that, the TM-polarized light is separated from the TE-polarized light and simultaneously rotated by the bent directional coupler.

A SEM photo and magnified micrographs of a fabricated PSR based on a bent directional coupler are provided in Figs. 7(a) and 7(b). Figures 7(c) and 7(d) show the measured and simulated transmission responses at the Cross and Thru ports of the fabricated PSRs for the TE- and TM-polarized light inputs, respectively. For the TE-polarized light input, the insertion loss is lower than 0.3 dB, and the crosstalk value is lower than −20 dB in the wavelength range of 1530 – 1600 nm. For the TM-polarized light input, the TM-to-TE conversion loss is 0.135 dB at $\lambda = 1564$ nm, and the conversion loss is lower than 1 dB in the wavelength range of 1544 – 1585 nm. The

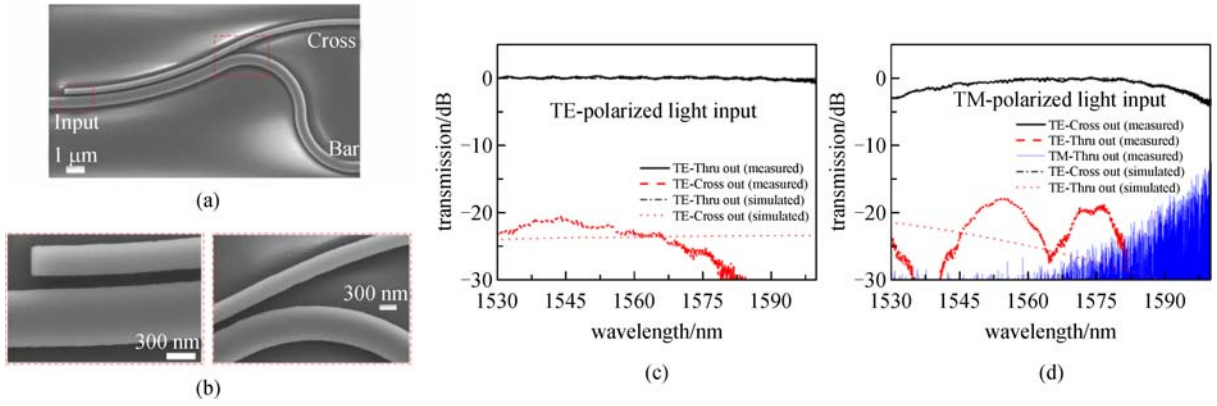

Fig. 7 (a) SEM photo of a fabricated PSR based on a bent directional coupler; (b) magnified micrographs of the bent directional coupler. Measured and simulated transmission responses at the Cross and Thru ports for (c) TE-polarization and (d) TM-polarization [45]

crosstalk value for the TM-polarized light input is < -18 dB. The residual TM-polarized light in the Thru port is depicted by the thin blue curve of Fig. 7(d). The blue field shows the noise of the remaining TM-polarized light in the Thru port at the longer wavelength, which is attributed to the fact that the wavelength is at the edge of the grating couplers' transmission spectra, resulting in large fluctuation of the normalized spectrum. The thin dashed curves in Figs. 7(c) and 7(d) represent the simulated responses of the PSR calculated by 3D-FDTD methods, which are in good agreement with the experimental results.

2.2.2 Silicon PSR using subwavelength grating [46]

Most previously reported PSRs show limited PERs (< 20 dB) and are sensitive to fabrication errors [42]. Some fabrication-tolerant PSRs were demonstrated employing tapered directional couplers or taper-etched waveguides, at the cost of large footprints and complex fabrication process [43,47,48]. Subwavelength grating (SWG) is a periodic structure functioning as a homogenous medium, which provides a new approach to effectively tailor the refractive index by modifying the pitch, width and duty cycle of the grating structure [49]. In addition, with properly designed parameters, the phase-matching condition can be maintained if the SWG waveguide width changes with that of a strip waveguide, thus resulting in tolerance to fabrication errors. Here, Figs. 8(a) and 8(b) show schematic structure of a silicon PSR using a SWG-based directional coupler with high tolerance to waveguide widths. The widths of the SWG waveguide and the strip waveguide are carefully designed to satisfy the phase-matching condition for cross-polarization coupling. The TM-polarized light in the strip waveguide is evanescently coupled to the SWG waveguide and rotated to TE-polarized light simultaneously. Therefore the TE-polarized light outputs at the Cross port. While, the TE-polarized light goes through the strip waveguide without coupling and outputs at the Thru port. Thus, the TE- and TM-polarized lights are separated and rotated by the SWG-based directional coupler. We use a bent directional coupler to filter the residual TM-polarized light in the Thru port and achieve a high PER. By properly designing the pitch and duty cycle of the SWG waveguide, the mode effective indices of the SWG waveguide and the strip waveguide can vary equally if the waveguide widths fluctuate, therefore maintaining the phase-matching condition and resulting in high tolerance to waveguide width variations. Figures 8(c) and 8(d) show the simulated power distributions of the proposed structure for the TE- and TM-polarized light inputs, respectively. The simulation results indicate that polarization beam splitting and rotating can be achieved simultaneously in the structure.

Figures 9(a) – 9(c) depict the SEM photo of a fabricated PSR, the measured and simulated transmission responses at the Cross and Thru ports of the fabricated PSR when the TE- and TM- polarized lights are injected, respectively. For the TE-polarized input light, the insertion loss is < 1.0 dB, and the PER is higher than ~13 dB in the wavelength range of 1540 – 1580 nm. For the TM-polarized light input, the TM-TE conversion loss is < 1.5 dB, and the PER is higher than ~19 dB in the wavelength range of 1507 – 1580 nm. To test the tolerance to waveguide width variation (ΔWG), the measured transmissions of the PSRs with ΔWG of $+ 50$ and $- 50$ nm are depicted in Fig. 9(d). For the TE-polarized light input, the insertion loss is < 1.0 dB, and the overall PER is higher than ~13 dB in the wavelength range of 1540 – 1580 nm. While, for the TM-polarized light input, the TM-TE conversion loss is < 3.3 dB, and the PER is higher than ~14 dB. These results show the large tolerance to waveguide width variations.

3 Silicon mode multiplexing devices

MDM is a promising solution to scale optical bandwidth by employing the spatial modes of on-chip waveguides [50].

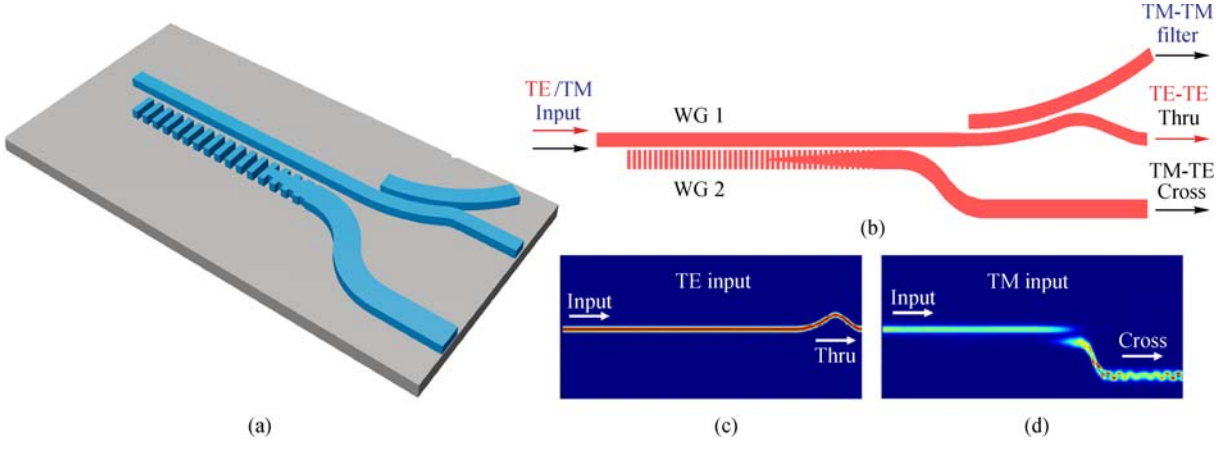

Fig. 8 Schematic structure of the SWG-PSR. (a) 3D view; (b) top view. Simulated power distributions of the SWG-PSR for (c) TE- and (d) TM-polarized light input, respectively [46]

Mode (de)multiplexers are key devices in the MDM schemes. Several schemes have been proposed to realize on-chip mode multiplexers, such as adiabatic mode-evolution coupler [51], asymmetric Y-junction [52], and asymmetric directional coupler [53]. The 3D view of the proposed SWG-based three- mode (de)multiplexer is sketched in Fig. 10(a). It consists of a bus waveguide and two SWG access waveguides. The TE_0 mode is injected

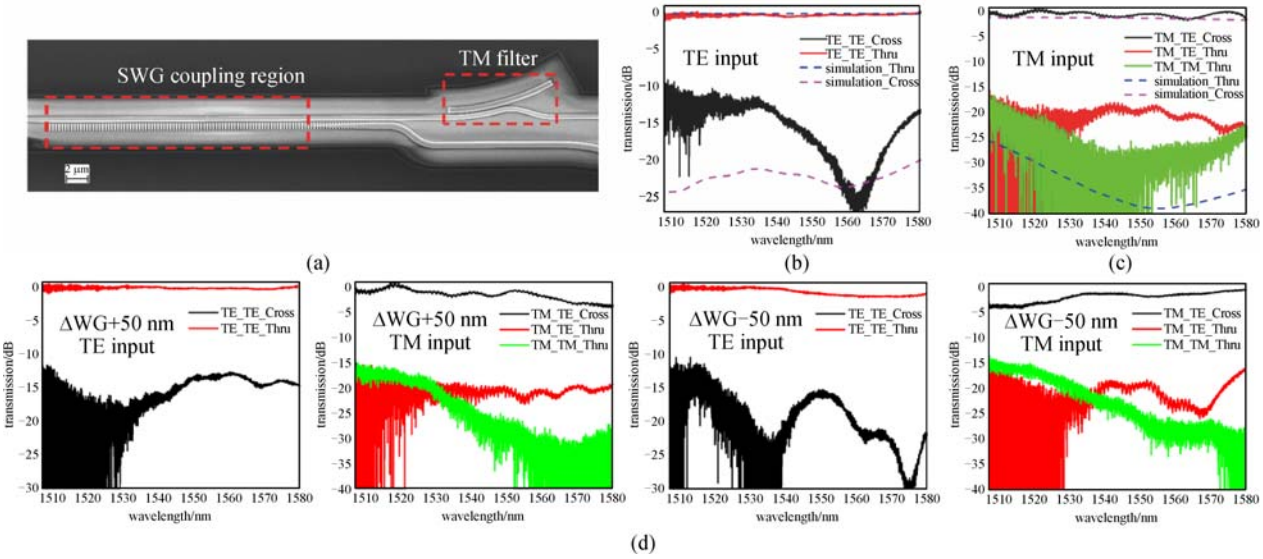

Fig. 9 (a) SEM photo of a fabricated PSR. Measured and simulated transmission responses for (b) TE-polarized and (c) TM-polarized light inputs, respectively. (d) Measured transmission responses of the PSRs with ΔWG of + 50 and −50 nm [46]

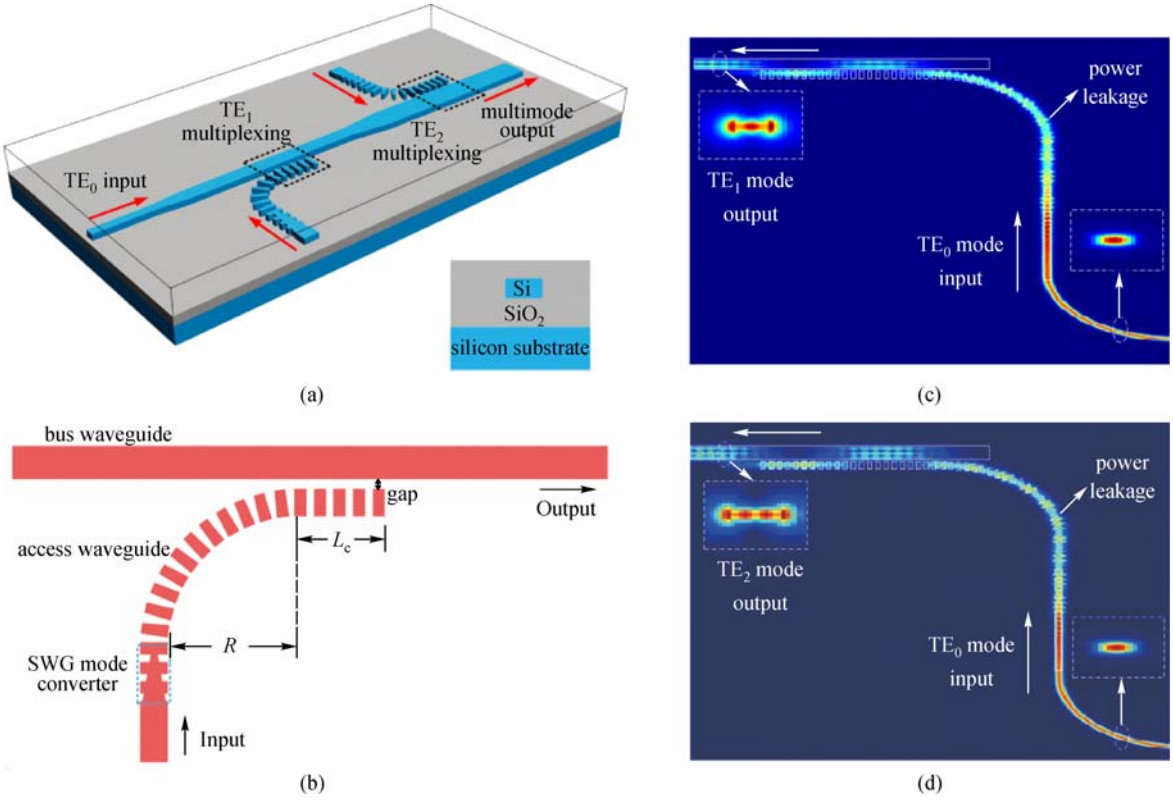

Fig. 10 Schematic structure of the proposed SWG-based mode multiplexer. (a) 3D view; (b) top view of the SWG-based directional coupler. Simulated power distributions of the SWG-based directional couplers for (c) TE_1 and (d) TE_2 modes multiplexing, respectively [54]

from the input port of the bus waveguide. The multiplexing of the higher-order modes (TE_1, TE_2 modes) are achieved by using the SWG-based directional coupler, as shown in Fig. 10(b). The simulated power distributions in the proposed SWG-based directional couplers are illustrated in Figs. 10(c) and 10(d). When the TE_0 modes are injected from the input ports of the SWG access waveguides, high efficient TE_1 or TE_2 modes are obtained at the output ports of the bus waveguides with different widths.

Figures 11(a)–11(c) show SEM photos of a fabricated mode multiplexer device. The footprint of the three-mode multiplexer is less than 88 μm × 20 μm. Figure 11(d) shows the measured transmission responses and modal crosstalk values of the fabricated mode (de)multiplexers. It can be seen that the signal outputs from the corresponding output port. For example, when the light inputs at port I_1, the signal outputs from the port O_1. The insertion loss is 0.8 dB and the crosstalk values are < -18 dB at 1550 nm for the TE_0 channel. For the TE_1 and TE_2 channels, the insertion losses are relatively high. This is mainly caused by introducing the bend SWG waveguides. We measured the performance of the SWG bend structure, the average bend loss is about 1.25 dB per 90°, while the coupling losses between the SWG access waveguides and the multimode bus waveguide are lower than 1 dB. For all the three channels, the overall insertion losses are lower than 3.8 dB, and the crosstalk values are below −16.3 dB at 1550 nm. The losses can be further reduced by optimizing the SWG parameters to minimize the bend scattering.

4 Mode and polarization selective switch

The switching and routing of data signals are basic requirements in network nodes. In analogy to a conventional wavelength selective switch (WSS) that routes any wavelength channel from one input port to any output port [55], a switch that can route mode- and polarization-multiplexed signals can effectively increase the capacity

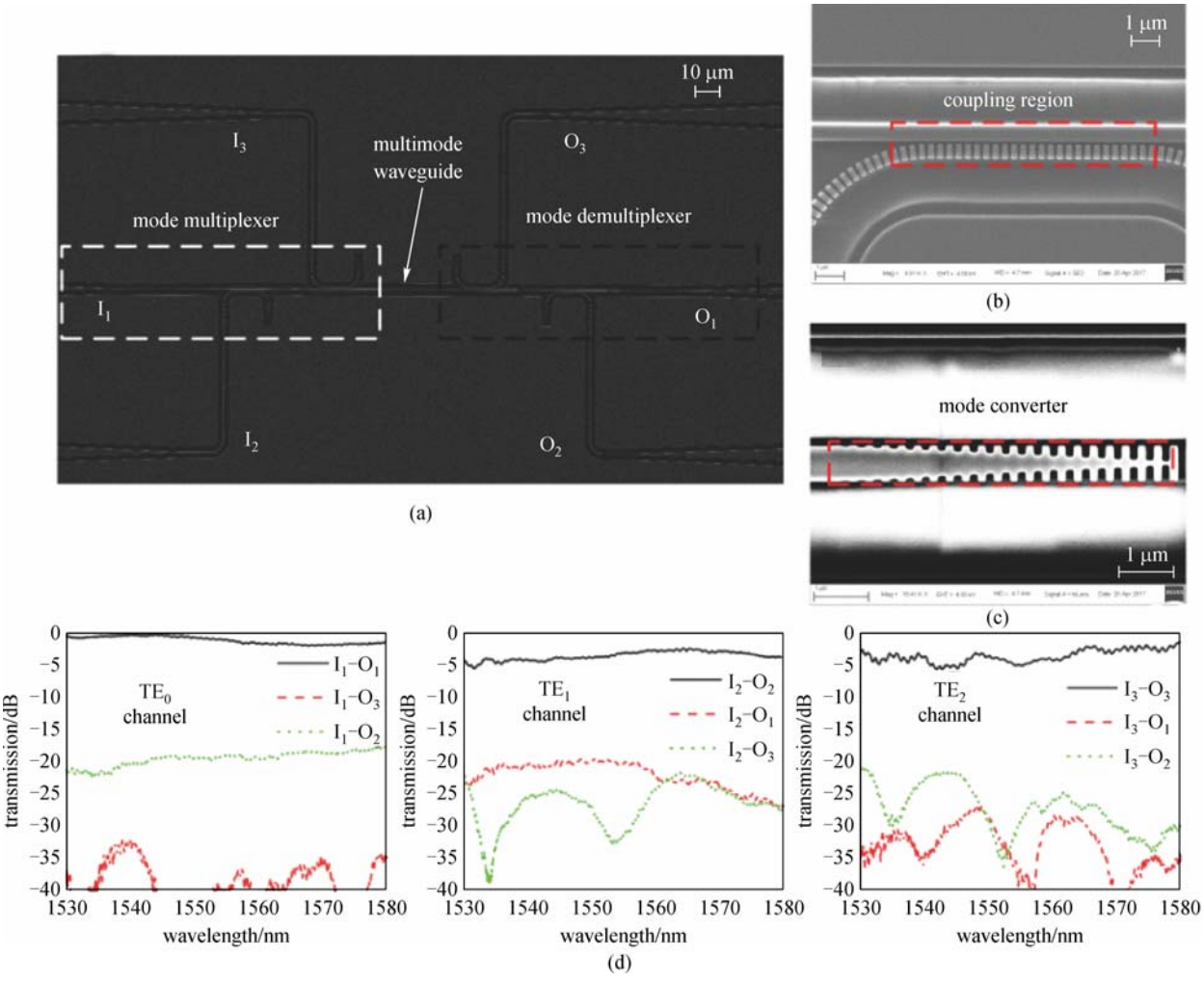

Fig. 11 (a)–(c) SEM photos of a fabricated SWG-based three-mode (de)multiplexer; (d) measured transmission responses at output ports O_i (i = 1, 2, 3) with the light input from port I_1, I_2, I_3, respectively [54]

and add new functionalities. A 4-channel silicon switch that used MDM signals on different wavelengths was achieved with crosstalk values of < -16.8 dB [56]. Recently, we demonstrated an on-chip silicon 1×2 mode- and polarization-selective switch on the same wavelength with crosstalk values of < -15 dB [57]. These reported crosstalk values need to be reduced to realize error-free switching in practical systems. The power penalty originated from the crosstalk is modulation format dependent [58,59], and typically at least 20-dB suppression ratio is needed between different modes and polarizations [60]. Moreover, these silicon mode- and polarization-switches are in 1×2 configurations, while 2×2 switches are desired as the fundamental building blocks of a general $N \times N$ switch fabric [61].

Figure 12 shows the schematic structure of the on-chip silicon 2×2 MPSS for 2 modes and 2 polarizations, which can route 4 channels of TE_0, TE_1, TM_0 and TM_1 modes. The routing of the channels is realized by the fundamental mode switches. The proposed 2×2 MPSS chip consists of 4 mode (de)multiplexers, 10 PBSs, 8 thermo-optic Mach-Zehnder interferometer (MZI) switches, 8 1×2 MMI couplers, 2 PBCs (polarization beam combiners) and 40 waveguide crossings. The mode multiplexer and the PBS are realized by cascaded directional couplers [53].

Figure 13 shows the microscope and SEM photos of a fabricated MPSS chip and element devices. The footprint of the MPSS device is less than 1.6 mm $\times$ 1.7 mm. The measured transmission spectra of the MPSS device are shown in Fig. 14. Take the TE_0 channel at input port I_1 as an example, the signal is switched to output port O_1 when the MZI heating power is 10.45 mW, and the signal is routed to output port O_2 when the applied heating power is 25.76 mW. For all the other channels, optical signals from different input ports can be routed to arbitrary output ports independently by applying different powers on the corresponding MZI switches, respectively. The overall insertion losses are lower than 8.6 dB at 1550 nm for all the channels. The inter-modal crosstalk is a critical challenge toward realizing error-free switching in practical systems. We measured the inter-modal crosstalk between channels by launching a signal to a fixed input port and measuring the transmission responses at each output port one by one, as shown in Fig. 14. The MZI switches were set to ensure the maximum output powers at the same output port. The measured inter-modal crosstalk values are lower than -23.2 dB for all the channels at 1550 nm. We further measured the intra-modal crosstalk values introduced by the MZI switches, as shown in Fig. 15. For the TE_0 channel of I_1 port, the intra-modal crosstalk values are lower than -26.6 dB at 1550 nm. For all the channels, the overall intra-modal crosstalk values are below -22.8 dB at 1550 nm. The total power consumption is about 200 mW when all the eight channels are switched on. Lower power consumption can be achieved by using suspended MZI switches [63].

We experimentally demonstrate the performance of the on-chip MPSS using the intensity modulated-direct detection (IM-DD) transmission scheme, with the setup shown in Fig. 16(a). A continuous wave light at 1550 nm is launched into a 25-GHz Mach-Zehnder modulator (MZM) (FTM7939EK), which is driven by an electrical 40-GSa/s

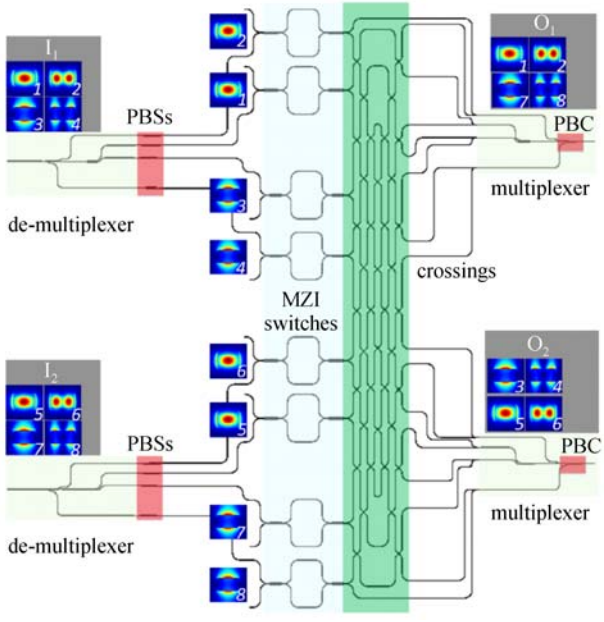

Fig. 12 Schematic structure of the 2×2 MPSS for 2 modes and 2 polarizations. As an example, the TE_0 and TE_1 channels of Input 1 and the TM_0 and TM_1 channels of Input 2 are routed to Output 1 and other channels are routed to Output 2 [62]

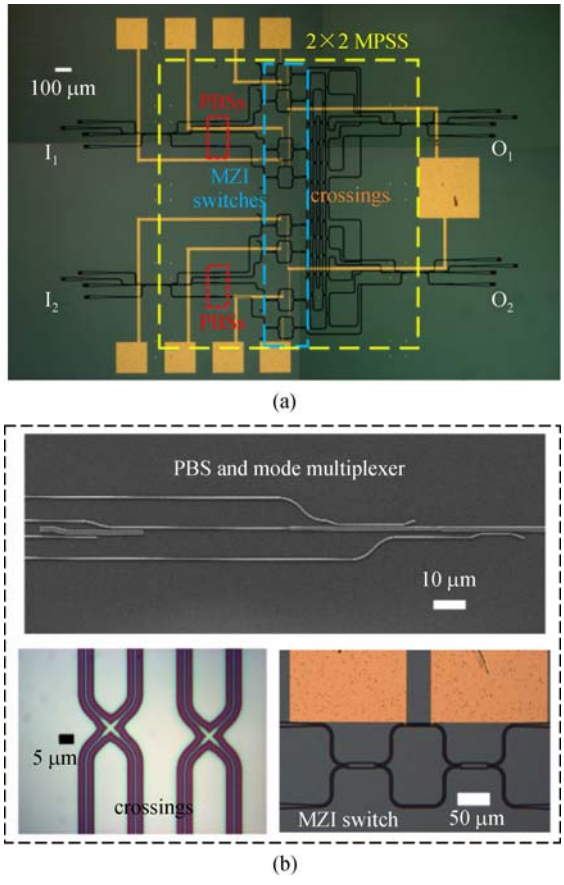

Fig. 13 (a) Microscope photo of a fabricated MPSS chip; (b) magnified SEM images and microscope photos of a PBS, a mode multiplexer, waveguide crossings and a MZI switch [62]

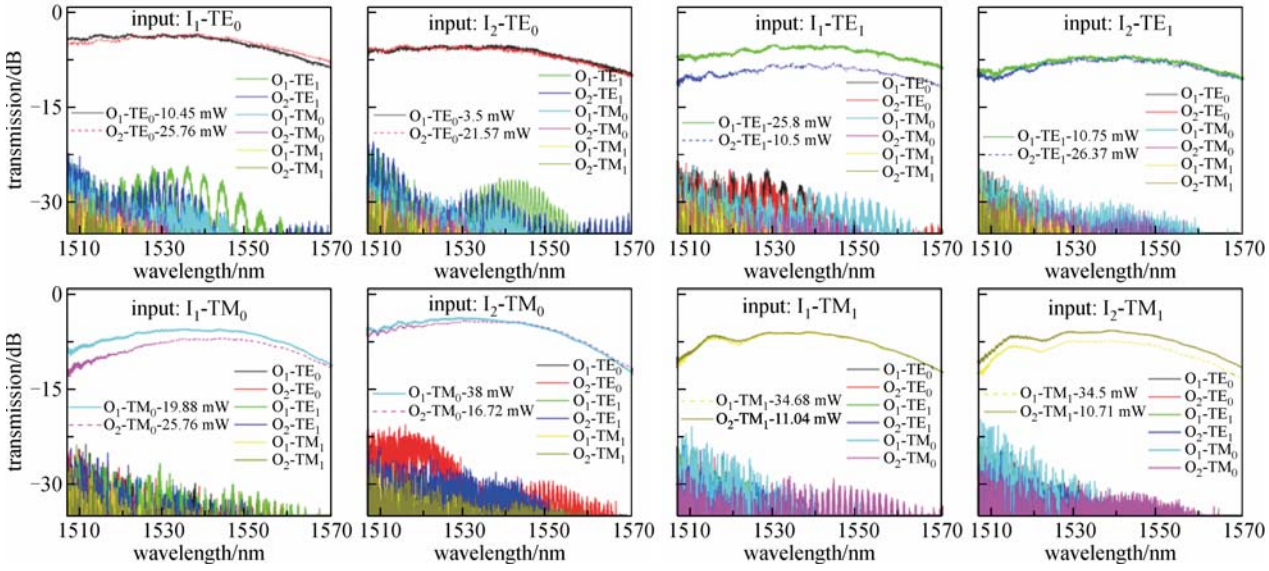

Fig. 14 Measured inter-modal crosstalk performances [62]

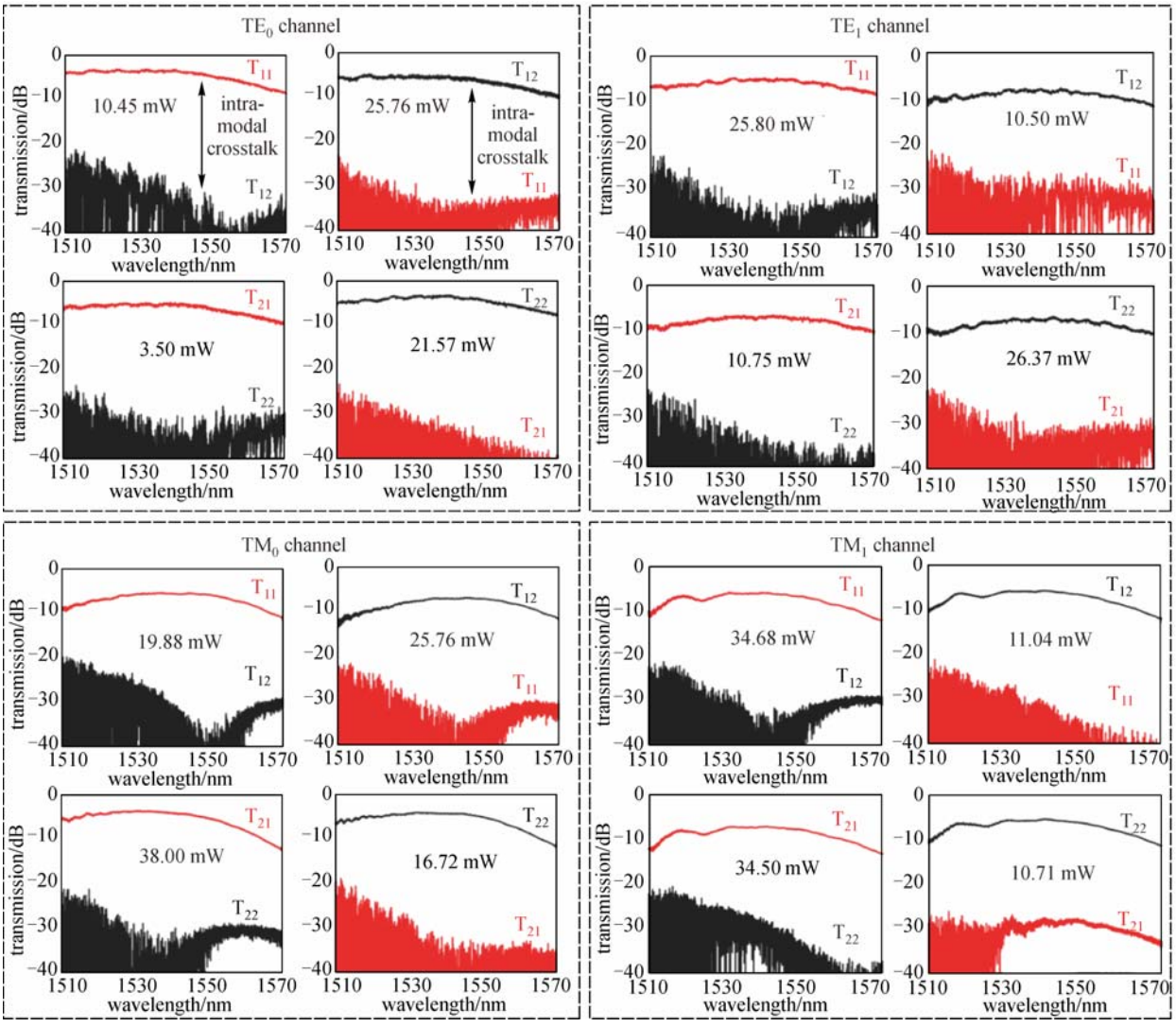

Fig. 15 Measured intra-modal crosstalk performances [62]

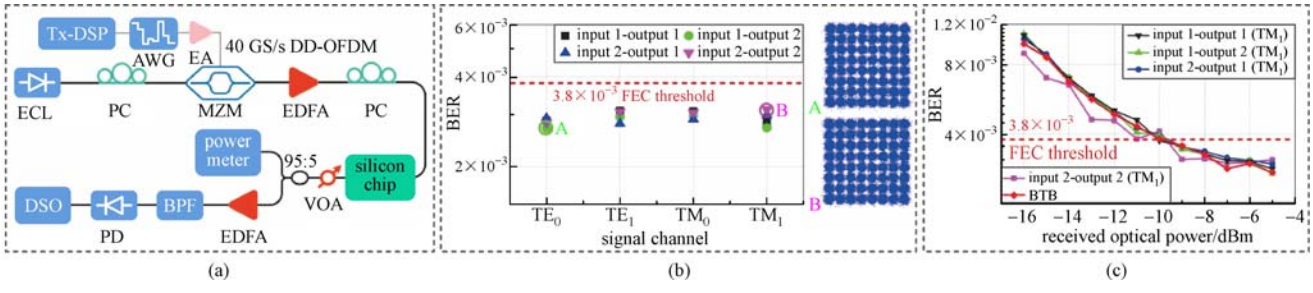

Fig. 16 (a) Experimental setup. ECL: external cavity laser. PC: polarization controller. MZM: Mach-Zehnder modulator. Tx-DSP: transmitter-digital signal processor. AWG: arbitrary waveform generator. EA: electrical amplifier. EDFA: erbium-doped fiber amplifier. VOA: variable optical attenuator. BPF: bandpass filter. PD: photodetector. DSO: digital storage oscilloscope. (b) BER versus channel. (c) BER curves versus received optical power [64]

intensity modulation-direct detection orthogonal frequency division multiplexed (IM-DD-OFDM) signal. An arbitrary waveform generator (AWG) (Keysight M8195A) generates the OFDM signal with a resampling rate of 60 GSa/s, and is followed by a linear driver. The output signal of the MZM is amplified by an erbium doped fiber amplifier (EDFA) and injected into the MPSS by grating couplers. Due to the lack of a fiber array, we tested one input and one output port at a time. On-chip optical signal switching is achieved. Subsequently, the output signal is coupled out, amplified, filtered, detected by a 40-GHz photodetector (XPDV2120R) and sampled by an 80-GSa/s digital storage oscilloscope (Lecroy LabMaster 10-36Zi-A). For the digital signal processing (DSP) at the transceivers, overheads of 0.1%, 3.7%, 1.9%, 1.5%, 2.9% are used for synchronization, equalization, cycle prefix, guard band at low frequency and optimization, respectively. Bit-loading is simultaneously realized with 64-, 32- and 16-QAM mapping and 64% subcarriers are allocated for 64-QAM. A raw data rate of 100.0 Gb/s is therefore realized. We measured the BERs of all the 16 possible configurations with a -5 dBm received power at the input port of the EDFA. As depicted in Fig. 16(b), similar performances are achieved, and the BERs are under the 7% forward error correction (FEC) threshold. Hence, the net data rate and the switching capacity of the MPSS are $100.0/(1+7\%) = 93.5$ Gb/s and $93.5 \times 2 \times 4 = 748$ Gb/s/λ, respectively. As seen in Fig. 16(c), negligible performance degradations are observed with the worst TM_1 channels [64].

5 Summary

We have reviewed our recent work on silicon polarization and mode handling devices. We demonstrated a high-extinction-ratio (>30 dB) grating-based PBS and a compact bridged-bent-coupler-based PBS. Then, we presented an ultra-compact bent-coupler-based (coupling length ~8.77 μm) PSR and a subwavelength-grating-based PSR with large tolerance to waveguide width variations. We also demonstrated a silicon three-mode (de)multiplexer employing SWG structure. Finally, we introduced an on-chip silicon 2×2 mode- and polarization-selective switches (MPSS) operating on one wavelength. The capacity of the switch can be further increased when combining with conventional WDM technology.

Acknowledgements We thank Prof. Richard Soref, Prof. Xiaoqing Jiang, Prof. Jianyi Yang, and Prof. Christine Tremblay et al. for their helpful discussion and contributions. This work was supported in part by the National Natural Science Foundation of China (NSFC) (Grant Nos. 61605112, 61235007, 61505104), in part by the 863 High-Tech Program (No. 2015AA017001), and in part by the Science and Technology Commission of Shanghai Municipality (Nos. 15ZR1422800, 16XD1401400). We thank the Center for Advanced Electronic Materials and Devices (AEMD) of Shanghai Jiao Tong University for the support in device fabrications.

References

1. Richardson D, Fini J, Nelson L. Space-division multiplexing in optical fibres. Nature Photonics, 2013, 7(5): 354–362
2. Winzer P J. Making spatial multiplexing a reality. Nature Photonics, 2014, 8(5): 345–348
3. Ding Y, Kamchevska V, Dalgaard K, Ye F, Asif R, Gross S, Withford M J, Galili M, Morioka T, Oxenløwe L K. Reconfigurable SDM switching using novel silicon photonic integrated circuit. Scientific Reports, 2016, 6(1): 39058
4. Bai N, Ip E, Huang Y K, Mateo E, Yaman F, Li M J, Bickham S, Ten S, Liñares J, Montero C, Moreno V, Prieto X, Tse V, Man Chung K, Lau A P T, Tam H Y, Lu C, Luo Y, Peng G D, Li G, Wang T. Mode-division multiplexed transmission with inline few-mode fiber amplifier. Optics Express, 2012, 20(3): 2668–2680
5. Ryf R, Randel S, Fontaine N K, Montoliu M, Burrows E, Chandrasekhar S, Gnauck A H, Xie C, Essiambre R J, Winzer P, Delbue R, Pupalaikis P, Sureka A, Sun Y, Gruner-Nielsen L, Jensen R V, Lingle R. 32-bit/s/Hz spectral efficiency WDM transmission over 177-km few-mode fiber. In: Proceedings of Optical Fiber Communication Conference/National Fiber Optic Engineers Conference. Optical Society of America, 2013, PDP5A.1
6. Thylén L, Wosinski L. Integrated photonics in the 21st century. Photonics Research, 2014, 2(2): 75–81
7. Soref R. Silicon photonics: a review of recent literature. Silicon, 2010, 2(1): 1–6
8. Gondarenko A, Levy J S, Lipson M. High confinement micron-scale silicon nitride high Q ring resonator. Optics Express, 2009, 17(14): 11366–11370
9. Chen P, Zhu Y, Shi Y, Dai D, He S. Fabrication and characterization of suspended SiO_2 ridge optical waveguides and the devices. Optics Express, 2012, 20(20): 22531–22536
10. Nozaki K, Tanabe T, Shinya A, Matsuo S, Sato T, Taniyama H, Notomi M. Sub-femtojoule all-optical switching using a photonic-crystal nanocavity. Nature Photonics, 2010, 4(7): 477–483
11. de Rossi A, Lauritano M, Combrié S, Tran Q V, Husko C. Interplay of plasma-induced and fast thermal nonlinearities in a GaAs-based photonic crystal nanocavity. Physical Review A, 2009, 79(4): 043818
12. Wang C, Burek M J, Lin Z, Atikian H A, Venkataraman V, Huang I C, Stark P, Lončar M. Integrated high quality factor lithium niobate microdisk resonators. Optics Express, 2014, 22(25): 30924–30933
13. Thomson D, Zilkie A, Bowers J E, Komljenovic T, Reed G T, Vivien L, Marris-Morini D, Cassan E, Virot L, Fédéli J M, Hartmann J M, Schmid J H, Xu D X, Boeuf F, O'Brien P, Mashanovich G Z, Nedeljkovic M. Roadmap on silicon photonics. Journal of Optics, 2016, 18(7): 073003
14. Liu J, Sun X, Camacho-Aguilera R, Kimerling L C, Michel J. Ge-on-Si laser operating at room temperature. Optics Letters, 2010, 35 (5): 679–681
15. Wirths S, Geiger R, von den Driesch N, Mussler G, Stoica T, Mantl S, Ikonic Z, Luysberg M, Chiussi S, Hartmann J M, Sigg H, Faist J, Buca D, Grützmacher D. Lasing in direct-bandgap GeSn alloy grown on Si. Nature Photonics, 2015, 9(2): 88–92

16. Zhang Y, Zeng C, Li D, Zhao X, Gao G, Yu J, Xia J. Enhanced light emission from Ge quantum dots in photonic crystal ring resonator. Optics Express, 2014, 22(10): 12248–12254
17. Zhang Y, Zeng C, Zhang H, Li D, Gao G, Huang Q, Wang Y, Yu J, Xia J. Single-mode emission from Ge quantum dots in photonic crystal nanobeam cavity. IEEE Photonics Technology Letters, 2015, 27(9): 1026–1029
18. Xu H, Xiao X, Li X, Hu Y, Li Z, Chu T, Yu Y, Yu J. High speed silicon Mach-Zehnder modulator based on interleaved PN junctions. Optics Express, 2012, 20(14): 15093–15099
19. Lu L, Zhao S, Zhou L, Li D, Li Z, Wang M, Li X, Chen J. 16 × 16 non-blocking silicon optical switch based on electro-optic Mach-Zehnder interferometers. Optics Express, 2016, 24(9): 9295–9307
20. Liu B, Zhang Y, He Y, Jiang X, Peng J, Qiu C, Su Y. Silicon photonic bandpass filter based on apodized subwavelength grating with high suppression ratio and short coupling length. Optics Express, 2017, 25(10): 11359–11364
21. Jiang X, Wu J, Yang Y, Pan T, Mao J, Liu B, Liu R, Zhang Y, Qiu C, Tremblay C, Su Y. Wavelength and bandwidth-tunable silicon comb filter based on Sagnac loop mirrors with Mach-Zehnder interferometer couplers. Optics Express, 2016, 24(3): 2183–2188
22. Jiang X, Yang Y, Zhang H, Peng J, Zhang Y, Qiu C, Su Y. Design and experimental demonstration of a compact silicon photonic interleaver based on an interfering loop with wide spectral range. Journal of Lightwave Technology, 2017, 35(17): 3765–3771
23. Zhang Y, Li D, Zeng C, Huang Z, Wang Y, Huang Q, Wu Y, Yu J, Xia J. Silicon optical diode based on cascaded photonic crystal cavities. Optics Letters, 2014, 39(6): 1370–1373
24. Chen G, Yu Y, Deng S, Liu L, Zhang X. Bandwidth improvement for germanium photodetector using wire bonding technology. Optics Express, 2015, 23(20): 25700–25706
25. Wang J, He S, Dai D. On-chip silicon 8-channel hybrid (de) multiplexer enabling simultaneous mode- and polarization-division-multiplexing. Laser & Photonics Reviews, 2014, 8(2): L18–L22
26. Dai D, Bauters J, Bowers J E. Passive technologies for future large-scale photonic integrated circuits on silicon: polarization handling, light non-reciprocity and loss reduction. Light, Science & Applications, 2012, 1(3): e1
27. Doerr C R, Chen L, Vermeulen D, Nielsen T, Azemati S, Stulz S, McBrien G, Xu X M, Mikkelsen B, Givehchi M, Rasmussen C, Park S Y. Single-chip silicon photonics 100-Gb/s coherent transceiver. In: Proceedings of Optical Fiber Communication Conference. Optical Society of America, 2014, Th5C.1
28. Dong P, Liu X, Sethumadhavan C, Buhl L L, Aroca R, Baeyens Y, Chen Y K. 224-Gb/s PDM-16-QAM modulator and receiver based on silicon photonic integrated circuits. In: Proceedings of Optical Fiber Communication Conference/National Fiber Optic Engineers Conference. Optical Society of America, 2013, PDP5C.6
29. Rahman B, Somasiri N, Themistos C, Grattan K. Design of optical polarization splitters in a single-section deeply etched MMI waveguide. Applied Physics B, Lasers and Optics, 2001, 73(5–6): 613–618
30. Ding Y, Ou H, Peucheret C. Wideband polarization splitter and rotator with large fabrication tolerance and simple fabrication process. Optics Letters, 2013, 38(8): 1227–1229
31. Ao X, Liu L, Wosinski L, He S. Polarization beam splitter based on a two-dimensional photonic crystal of pillar type. Applied Physics Letters, 2006, 89(17): 171115
32. Feng J, Zhou Z. Polarization beam splitter using a binary blazed grating coupler. Optics Letters, 2007, 32(12): 1662–1664
33. Chu H S, Li E P, Bai P, Hegde R. Optical performance of single-mode hybrid dielectric-loaded plasmonic waveguide-based components. Applied Physics Letters, 2010, 96(22): 221103
34. Guan X, Wu H, Shi Y, Dai D. Extremely small polarization beam splitter based on a multimode interference coupler with a silicon hybrid plasmonic waveguide. Optics Letters, 2014, 39(2): 259–262
35. Fukuda H, Yamada K, Tsuchizawa T, Watanabe T, Shinojima H, Itabashi S. Ultrasmall polarization splitter based on silicon wire waveguides. Optics Express, 2006, 14(25): 12401–12408
36. Dai D, Bowers J E. Novel ultra-short and ultra-broadband polarization beam splitter based on a bent directional coupler. Optics Express, 2011, 19(19): 18614–18620
37. Zhang Y, He Y, Wu J, Jiang X, Liu R, Qiu C, Jiang X, Yang J, Tremblay C, Su Y. High-extinction-ratio silicon polarization beam splitter with tolerance to waveguide width and coupling length variations. Optics Express, 2016, 24(6): 6586–6593
38. Kim D W, Lee M H, Kim Y, Kim K H. Planar-type polarization beam splitter based on a bridged silicon waveguide coupler. Optics Express, 2015, 23(2): 998–1004
39. Qiu H, Su Y, Yu P, Hu T, Yang J, Jiang X. Compact polarization splitter based on silicon grating-assisted couplers. Optics Letters, 2015, 40(9): 1885–1887
40. Zhang Y, He Y, Jiang X, Liu B, Qiu C, Su Y. Ultra-compact broadband silicon polarization beam splitter based on a bridged bent directional coupler. In: Proceedings of IEEE 13th International Conference on Group IV Photonics (GFP). IEEE Photonics Society, 2016, ThP18
41. Liu L, Ding Y, Yvind K, Hvam J M. Efficient and compact TE-TM polarization converter built on silicon-on-insulator platform with a simple fabrication process. Optics Letters, 2011, 36(7): 1059–1061
42. Liu L, Ding Y, Yvind K, Hvam J M. Silicon-on-insulator polarization splitting and rotating device for polarization diversity circuits. Optics Express, 2011, 19(13): 12646–12651
43. Tan K, Huang Y, Lo G Q, Yu C, Lee C. Ultra-broadband fabrication-tolerant polarization splitter and rotator. In: Proceedings of Optical Fiber Communication Conference. Optical Society of America, 2017, Th1G.7
44. Wang J, Niu B, Sheng Z, Wu A, Li W, Wang X, Zou S, Qi M, Gan F. Novel ultra-broadband polarization splitter-rotator based on mode-evolution tapers and a mode-sorting asymmetric Y-junction. Optics Express, 2014, 22(11): 13565–13571
45. Zhang Y, He Y, Jiang X, Liu B, Qiu C, Su Y, Soref R A. Ultra-compact and highly efficient silicon polarization splitter and rotator. APL Photonics, 2016, 1(9): 091304
46. He Y, Zhang Y, Wang X, Liu B, Jiang X, Qiu C, Su Y, Soref R. Silicon polarization splitter and rotator using a subwavelength grating based directional coupler. In: Proceedings of Optical Fiber Communication Conference. Optical Society of America, 2017, Th1G.6
47. Ding Y, Liu L, Peucheret C, Ou H. Fabrication tolerant polarization splitter and rotator based on a tapered directional coupler. Optics Express, 2012, 20(18): 20021–20027

48. Xiong Y, Xu D X, Schmid J H, Cheben P, Janz S, Ye W N. Fabrication tolerant and broadband polarization splitter and rotator based on a taper-etched directional coupler. Optics Express, 2014, 22(14): 17458–17465
49. Halir R, Bock P J, Cheben P, Ortega-Moñux A, Alonso-Ramos C, Schmid J H, Lapointe J, Xu D X, Wangüemert‐Pérez J G, Molina-Fernández Í, Janz S. Waveguide sub-wavelength structures: a review of principles and applications. Laser & Photonics Reviews, 2015, 9 (1): 25–49
50. Xing J, Li Z, Xiao X, Yu J, Yu Y. Two-mode multiplexer and demultiplexer based on adiabatic couplers. Optics Letters, 2013, 38 (17): 3468–3470
51. Riesen N, Love J D. Design of mode-sorting asymmetric Y-junctions. Applied Optics, 2012, 51(15): 2778–2783
52. Dai D, Wang J, Shi Y. Silicon mode (de)multiplexer enabling high capacity photonic networks-on-chip with a single-wavelength-carrier light. Optics Letters, 2013, 38(9): 1422–1424
53. Luo L W, Ophir N, Chen C P, Gabrielli L H, Poitras C B, Bergmen K, Lipson M. WDM-compatible mode-division multiplexing on a silicon chip. Nature Communications, 2014, 5: 3069
54. He Y, Zhang Y, Jiang X, Qiu C, Su Y. On-chip silicon three-mode (de)multiplexer employing subwavelength grating structure. In: Proceedings of 43nd European Conference on Optical Communication . ECOC, 2017, W2C.3
55. Doerr C R, Buhl L, Chen L, Dupuis N. Monolithic gridless 1 × 2 wavelength-selective switch in silicon. In: Proceedings of Optical Fiber Communication Conference/National Fiber Optic Engineers Conference. Optical Society of America, 2011, PDPC4
56. Stern B, Zhu X, Chen C P, Tzuang L D, Cardenas J, Bergman K, Lipson M. On-chip mode-division multiplexing switch. Optica, 2015, 2(6): 530–535
57. Zhang Y, Zhu Q, He Y, Qiu C, Su Y, Soref R. Silicon 1 × 2 mode- and polarization-selective switch. In: Proceedings of Optical Fiber Communication Conference. Optical Society of America, 2017, W4E.2
58. Winzer P, Gnauck A, Konczykowska A, Jorge F, Dupuy J Y. Penalties from in-band crosstalk for advanced optical modulation formats. In: Proceedings of 37th European Conference and Exposition on Optical Communications. ECOC, 2011, Tu.5.B.7
59. Ding Y, Xu J, Da Ros F, Huang B, Ou H, Peucheret C. On-chip two-mode division multiplexing using tapered directional coupler-based mode multiplexer and demultiplexer. Optics Express, 2013, 21(8): 10376–10382
60. Downie J D, Ruffin A B. Analysis of signal distortion and crosstalk penalties induced by optical filters in optical networks. Journal of Lightwave Technology, 2003, 21(9): 1876–1886
61. Poon A W, Luo X, Xu F, Chen H. Cascaded microresonator-based matrix switch for silicon on-chip optical interconnection. Proceedings of the IEEE, 2009, 97(7): 1216–1238
62. Zhang Y, He Y, Zhu Q, Qiu C, Su Y. On-chip silicon photonic 2×2 mode- and polarization-selective switch with low inter-modal crosstalk. Photonics Research, 2017, 5(5): 521–526
63. Fang Q, Song J F, Liow T Y, Cai H, Yu M B, Lo G Q, Kwong D L. Ultralow power silicon photonics thermo-optic switch with suspended phase arms. IEEE Photonics Technology Letters, 2011, 23(8): 525–527
64. Zhu Q M, Zhang Y, He Y, An S H, Qiu C Y, Guo X H, Su Y K. On-chip switching of mode- and polarization-multiplexed signals with a 748-Gb/s/λ (8×93.5-Gb/s) capacity. In: Proceedings of CLEO, 2018, accepted

Yong Zhang received the B.S. degree from Northwestern Polytechnical University, Xi'an, China in 2010, and the Ph.D. degree from Huazhong University of Science and Technology, Wuhan, China, in 2015. He joined Shanghai Jiao Tong University, Shanghai, China, as an assistant professor in July 2015. His research interests include silicon photonics devices, polarization and mode devices, microcavity devices, e-beam lithography and ICP etching process. Dr. Zhang has published over 40 journal and conference papers, including *Optics Letters*, *Optics Express*, *APL Photonics*, and OFC/ ECOC/CLEO conferences and etc. Dr. Zhang served as an editorial board member of *Laser Research & Applications* (2017–), a guest editor of *Science China Information Sciences* (2017), and a guest editor of *International Journal of Optics* (2017). He was the treasurer (2017–) and the secretary (2016–2017) of IEEE Photonics Society Shanghai chapter. He also served as a TPC member of international conferences including SOPO (2017) and IWWCN (2017). Dr. Zhang is a member of IEEE and OSA.

Yu He received the B.S. degree from Nankai University, Tianjin, China, in 2015. He is currently working toward the Ph.D. degree at Shanghai Jiao Tong University, Shanghai, China. His research interests include silicon photonics devices and circuit, polarization handling devices and wavelength/mode multiplexing devices.

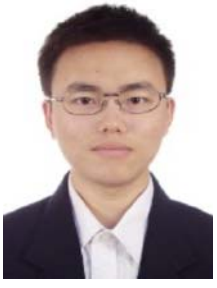

Qingming Zhu received the B.S. degree from Southeast University, Nanjing, China, in 2015. He is currently working toward the Ph.D. degree at Shanghai Jiao Tong University, Shanghai, China. His current research interests include silicon microring switch and high-speed transmission system.

Xinhong Jiang received the B.S. and M.S. degrees from Anhui University, Hefei, China, in 2009 and 2012, respectively. He is currently working toward the Ph.D. degree at Shanghai Jiao Tong University, Shanghai, China. His current research interests include silicon photonics, optical filters and switches.

Xuhan Guo (M'17) received the B.S. degree from Huazhong University of Science and Technology, Wuhan, China in 2009 and the Ph.D. degree from the University of Cambridge, Cambridge, UK, in 2014. He has worked as a Research Associate in University of Cambridge until 2017, then he moved to Shanghai Jiao Tong University, China, where he is currently Associate Professor of Photonics. He is the author or co-author of more than 30 publications. His current research interests include hybrid silicon lasers, silicon photonics devices and circuit, PON. He also serves as a TPC member of a number of international conferences including ECOC (2018–), CLEO Pacific Rim (2018–), IEEE GLOBECOM (2016–2017), ECIO (2010), the secretary (2018–) of IEEE Photonics Society Shanghai chapter. Dr. Guo is a member of IEEE and a member of OSA.

Ciyuan Qiu received the B.S. and M.S. degrees from Tsinghua University, Beijing, China, in 2005 and 2007, respectively, and the Ph.D. degree from Rice University, Houston, TX, USA, in 2013. He then worked as Postdoc at Rice University until June 2014. He is currently an associate professor at Shanghai Jiao Tong University, Shanghai, China. His current research interests include silicon photonics devices and circuits, graphene optics, and plasmonics. He has been the author or coauthor of more than 60 journal articles and conference papers, such as *Nano Letters*, *Scientific Reports*, *Optics Letters*, and *Optics Express*. He is the vice president of IEEE Photonics Society Shanghai chapter. He also served as a TPC member of international conferences including ICOCN (2015) and OECC (2015, 2018).

Yikai Su (S'97–M'01–SM'07) received the B.S. degree from the Hefei University of Technology, China, in 1991, the M.S. degree from the Beijing University of Aeronautics and Astronautics (BUAA), China, in 1994, and the Ph.D. degree in EE from Northwestern University, Evanston, IL, USA in 2001. He worked at Crawford Hill Laboratory of Bell Laboratories before he joined the Shanghai Jiao Tong University, Shanghai, China, as a Full Professor in 2004. His research areas cover silicon photonic devices for information transmission and switching. He has over 300 publications in international journals and conferences, with more than 2100 citations (Scopus search). He holds 6 US patents and ~50 Chinese patents.

Prof. Su served as an advisory board member of *Advanced Optical Materials* and *Advanced Materials Technologies* (2015–), an associate editor of *APL Photonics* (2016–2018) and *Photonics Research* (2013–2016), a topical editor of *Optics Letters* (2008–2014), a guest editor of *IEEE JSTQE* (2008/2011), and a feature editor of *Applied Optics* (2008). He is the chair of IEEE Photonics Society Shanghai chapter, a general co-chair of ACP 2012, a TPC co-chair of ACP 2011 and APCC 2009. He also served as a TPC member of a large number of international conferences including CLEO (2016–), ECOC (2013–2016), OFC (2011–2013), OECC 2008, CLEO-PR 2007, and LEOS (2005–2007). Prof. Su is a senior member of IEEE and a member of OSA.